

Measurement of the $W^+W^-\gamma$ Cross-section and First Direct Limits on Anomalous Electroweak Quartic Gauge Couplings

The OPAL Collaboration

Abstract

A study of W^+W^- events accompanied by hard photon radiation produced in e^+e^- collisions at LEP is presented. Events consistent with two on-shell W-bosons and an isolated photon are selected from 183 pb^{-1} of data recorded at $\sqrt{s} = 189 \text{ GeV}$. From these data, 17 $W^+W^-\gamma$ candidates are selected with photon energy greater than 10 GeV, consistent with the Standard Model expectation. These events are used to measure the $e^+e^- \rightarrow W^+W^-\gamma$ cross-section within a set of geometric and kinematic cuts, $\hat{\sigma}_{WW\gamma} = 136 \pm 37 \pm 8 \text{ fb}$, where the first error is statistical and the second systematic. The photon energy spectrum is used to set the first direct, albeit weak, limits on possible anomalous contributions to the $W^+W^-\gamma\gamma$ and $W^+W^-\gamma Z^0$ vertices:

$$\begin{aligned} -0.070 \text{ GeV}^{-2} &< a_0/\Lambda^2 < 0.070 \text{ GeV}^{-2}, \\ -0.13 \text{ GeV}^{-2} &< a_c/\Lambda^2 < 0.19 \text{ GeV}^{-2}, \\ -0.61 \text{ GeV}^{-2} &< a_n/\Lambda^2 < 0.57 \text{ GeV}^{-2}, \end{aligned}$$

where Λ represents the energy scale for new physics.

The OPAL Collaboration

G. Abbiendi², K. Ackerstaff⁸, P.F. Akesson³, G. Alexander²³, J. Allison¹⁶, K.J. Anderson⁹,
S. Arcelli¹⁷, S. Asai²⁴, S.F. Ashby¹, D. Axen²⁹, G. Azuelos^{18,a}, I. Bailey²⁸, A.H. Ball⁸,
E. Barberio⁸, R.J. Barlow¹⁶, J.R. Batley⁵, S. Baumann³, T. Behnke²⁷, K.W. Bell²⁰, G. Bella²³,
A. Bellerive⁹, S. Bentvelsen⁸, S. Bethke^{14,i}, S. Betts¹⁵, O. Biebel^{14,i}, A. Biguzzi⁵,
I.J. Bloodworth¹, P. Bock¹¹, J. Böhme^{14,h}, O. Boeriu¹⁰, D. Bonacorsi², M. Boutemour³³,
S. Braibant⁸, P. Bright-Thomas¹, L. Brigliadori², R.M. Brown²⁰, H.J. Burckhart⁸,
P. Capiluppi², R.K. Carnegie⁶, A.A. Carter¹³, J.R. Carter⁵, C.Y. Chang¹⁷, D.G. Charlton^{1,b},
D. Chrisman⁴, C. Ciocca², P.E.L. Clarke¹⁵, E. Clay¹⁵, I. Cohen²³, J.E. Conboy¹⁵, O.C. Cooke⁸,
J. Couchman¹⁵, C. Couyoumtzelis¹³, R.L. Coxe⁹, M. Cuffiani², S. Dado²², G.M. Dallavalle²,
S. Dallison¹⁶, R. Davis³⁰, A. de Roeck⁸, P. Dervan¹⁵, K. Desch²⁷, B. Dienes^{32,h}, M.S. Dixit⁷,
M. Donkers⁶, J. Dubbert³³, E. Duchovni²⁶, G. Duckeck³³, I.P. Duerdoth¹⁶, P.G. Estabrooks⁶,
E. Etzion²³, F. Fabbri², A. Fanfani², M. Fanti², A.A. Faust³⁰, L. Feld¹⁰, P. Ferrari¹²,
F. Fiedler²⁷, M. Fierro², I. Fleck¹⁰, A. Frey⁸, A. Fürtjes⁸, D.I. Futyan¹⁶, P. Gagnon¹²,
J.W. Gary⁴, G. Gaycken²⁷, C. Geich-Gimbel³, G. Giacomelli², P. Giacomelli²,
D.M. Gingrich^{30,a}, D. Glenzinski⁹, J. Goldberg²², W. Gorn⁴, C. Grandi², K. Graham²⁸,
E. Gross²⁶, J. Grunhaus²³, M. Gruwé²⁷, C. Hajdu³¹, G.G. Hanson¹², M. Hansroul⁸, M. Hapke¹³,
K. Harder²⁷, A. Harel²², C.K. Hargrove⁷, M. Harin-Dirac⁴, M. Hauschild⁸, C.M. Hawkes¹,
R. Hawkings²⁷, R.J. Hemingway⁶, G. Herten¹⁰, R.D. Heuer²⁷, M.D. Hildreth⁸, J.C. Hill⁵,
P.R. Hobson²⁵, A. Hocker⁹, K. Hoffman⁸, R.J. Homer¹, A.K. Honma⁸, D. Horváth^{31,c},
K.R. Hossain³⁰, R. Howard²⁹, P. Hütemeyer²⁷, P. Igo-Kemenes¹¹, D.C. Imrie²⁵, K. Ishii²⁴,
F.R. Jacob²⁰, A. Jawahery¹⁷, H. Jeremie¹⁸, M. Jimack¹, C.R. Jones⁵, P. Jovanovic¹, T.R. Junk⁶,
N. Kanaya²⁴, J. Kanzaki²⁴, G. Karapetian¹⁸, D. Karlen⁶, V. Kartvelishvili¹⁶, K. Kawagoe²⁴,
T. Kawamoto²⁴, P.I. Kayal³⁰, R.K. Keeler²⁸, R.G. Kellogg¹⁷, B.W. Kennedy²⁰, D.H. Kim¹⁹,
A. Klier²⁶, T. Kobayashi²⁴, M. Kobel³, T.P. Kokott³, M. Kolrep¹⁰, S. Komamiya²⁴,
R.V. Kowalewski²⁸, T. Kress⁴, P. Krieger⁶, J. von Krogh¹¹, T. Kuhl³, M. Kupper²⁶, P. Kyberd¹³,
G.D. Lafferty¹⁶, H. Landsman²², D. Lanske¹⁴, J. Lauber¹⁵, I. Lawson²⁸, J.G. Layter⁴,
D. Lellouch²⁶, J. Letts¹², L. Levinson²⁶, R. Liebisch¹¹, J. Lillich¹⁰, B. List⁸, C. Littlewood⁵,
A.W. Lloyd¹, S.L. Lloyd¹³, F.K. Loebinger¹⁶, G.D. Long²⁸, M.J. Losty⁷, J. Lu²⁹, J. Ludwig¹⁰,
A. Macchiolo¹⁸, A. Macpherson³⁰, W. Mader³, M. Mannelli⁸, S. Marcellini², T.E. Marchant¹⁶,
A.J. Martin¹³, J.P. Martin¹⁸, G. Martinez¹⁷, T. Mashimo²⁴, P. Mättig²⁶, W.J. McDonald³⁰,
J. McKenna²⁹, E.A. Mckigney¹⁵, T.J. McMahon¹, R.A. McPherson²⁸, F. Meijers⁸,
P. Mendez-Lorenzo³³, F.S. Merritt⁹, H. Mes⁷, I. Meyer⁵, A. Michelini², S. Mihara²⁴,
G. Mikenberg²⁶, D.J. Miller¹⁵, W. Mohr¹⁰, A. Montanari², T. Mori²⁴, K. Nagai⁸, I. Nakamura²⁴,
H.A. Neal^{12,f}, R. Nisius⁸, S.W. O’Neale¹, F.G. Oakham⁷, F. Odorici², H.O. Ogren¹²,
A. Okpara¹¹, M.J. Oreglia⁹, S. Orito²⁴, G. Pásztor³¹, J.R. Pater¹⁶, G.N. Patrick²⁰, J. Patt¹⁰,
R. Perez-Ochoa⁸, S. Petzold²⁷, P. Pfeifenschneider¹⁴, J.E. Pilcher⁹, J. Pinfold³⁰, D.E. Plane⁸,
B. Poli², J. Polok⁸, M. Przybycień^{8,d}, A. Quadt⁸, C. Rembser⁸, H. Rick⁸, S.A. Robins²²,
N. Rodning³⁰, J.M. Roney²⁸, S. Rosati³, K. Roscoe¹⁶, A.M. Rossi², Y. Rozen²², K. Runge¹⁰,
O. Runolfsson⁸, D.R. Rust¹², K. Sachs¹⁰, T. Saeki²⁴, O. Sahr³³, W.M. Sang²⁵,
E.K.G. Sarkisyan²³, C. Sbarra²⁸, A.D. Schaile³³, O. Schaile³³, P. Scharff-Hansen⁸, J. Schieck¹¹,
S. Schmitt¹¹, A. Schöning⁸, M. Schröder⁸, M. Schumacher³, C. Schwick⁸, W.G. Scott²⁰,
R. Seuster^{14,h}, T.G. Shears⁸, B.C. Shen⁴, C.H. Shepherd-Themistocleous⁵, P. Sherwood¹⁵,
G.P. Siroli², A. Skuja¹⁷, A.M. Smith⁸, G.A. Snow¹⁷, R. Sobie²⁸, S. Söldner-Rembold^{10,e},
S. Spagnolo²⁰, M. Sproston²⁰, A. Stahl³, K. Stephens¹⁶, K. Stoll¹⁰, D. Strom¹⁹, R. Ströhmer³³,

B. Surrow⁸, S.D. Talbot¹, P. Taras¹⁸, S. Tarem²², R. Teuscher⁹, M. Thiergen¹⁰, J. Thomas¹⁵,
M.A. Thomson⁸, E. Torrence⁸, S. Towers⁶, T. Trefzger³³, I. Trigger¹⁸, Z. Trócsányi^{32,g},
E. Tsur²³, M.F. Turner-Watson¹, I. Ueda²⁴, R. Van Kooten¹², P. Vannerem¹⁰, M. Verzocchi⁸,
H. Voss³, F. Wäckerle¹⁰, D. Waller⁶, C.P. Ward⁵, D.R. Ward⁵, P.M. Watkins¹, A.T. Watson¹,
N.K. Watson¹, P.S. Wells⁸, T. Wengler⁸, N. Wermes³, D. Wetterling¹¹, J.S. White⁶,
G.W. Wilson¹⁶, J.A. Wilson¹, T.R. Wyatt¹⁶, S. Yamashita²⁴, V. Zacek¹⁸, D. Zer-Zion⁸

¹School of Physics and Astronomy, University of Birmingham, Birmingham B15 2TT, UK

²Dipartimento di Fisica dell' Università di Bologna and INFN, I-40126 Bologna, Italy

³Physikalisches Institut, Universität Bonn, D-53115 Bonn, Germany

⁴Department of Physics, University of California, Riverside CA 92521, USA

⁵Cavendish Laboratory, Cambridge CB3 0HE, UK

⁶Ottawa-Carleton Institute for Physics, Department of Physics, Carleton University, Ottawa, Ontario K1S 5B6, Canada

⁷Centre for Research in Particle Physics, Carleton University, Ottawa, Ontario K1S 5B6, Canada

⁸CERN, European Organisation for Particle Physics, CH-1211 Geneva 23, Switzerland

⁹Enrico Fermi Institute and Department of Physics, University of Chicago, Chicago IL 60637, USA

¹⁰Fakultät für Physik, Albert Ludwigs Universität, D-79104 Freiburg, Germany

¹¹Physikalisches Institut, Universität Heidelberg, D-69120 Heidelberg, Germany

¹²Indiana University, Department of Physics, Swain Hall West 117, Bloomington IN 47405, USA

¹³Queen Mary and Westfield College, University of London, London E1 4NS, UK

¹⁴Technische Hochschule Aachen, III Physikalisches Institut, Sommerfeldstrasse 26-28, D-52056 Aachen, Germany

¹⁵University College London, London WC1E 6BT, UK

¹⁶Department of Physics, Schuster Laboratory, The University, Manchester M13 9PL, UK

¹⁷Department of Physics, University of Maryland, College Park, MD 20742, USA

¹⁸Laboratoire de Physique Nucléaire, Université de Montréal, Montréal, Quebec H3C 3J7, Canada

¹⁹University of Oregon, Department of Physics, Eugene OR 97403, USA

²⁰CLRC Rutherford Appleton Laboratory, Chilton, Didcot, Oxfordshire OX11 0QX, UK

²²Department of Physics, Technion-Israel Institute of Technology, Haifa 32000, Israel

²³Department of Physics and Astronomy, Tel Aviv University, Tel Aviv 69978, Israel

²⁴International Centre for Elementary Particle Physics and Department of Physics, University of Tokyo, Tokyo 113-0033, and Kobe University, Kobe 657-8501, Japan

²⁵Institute of Physical and Environmental Sciences, Brunel University, Uxbridge, Middlesex UB8 3PH, UK

²⁶Particle Physics Department, Weizmann Institute of Science, Rehovot 76100, Israel

²⁷Universität Hamburg/DESY, II Institut für Experimental Physik, Notkestrasse 85, D-22607 Hamburg, Germany

²⁸University of Victoria, Department of Physics, P O Box 3055, Victoria BC V8W 3P6, Canada

²⁹University of British Columbia, Department of Physics, Vancouver BC V6T 1Z1, Canada

³⁰University of Alberta, Department of Physics, Edmonton AB T6G 2J1, Canada

³¹Research Institute for Particle and Nuclear Physics, H-1525 Budapest, P O Box 49, Hungary

³²Institute of Nuclear Research, H-4001 Debrecen, P O Box 51, Hungary

³³Ludwigs-Maximilians-Universität München, Sektion Physik, Am Coulombwall 1, D-85748 Garching, Germany

^a and at TRIUMF, Vancouver, Canada V6T 2A3

^b and Royal Society University Research Fellow

^c and Institute of Nuclear Research, Debrecen, Hungary

^d and University of Mining and Metallurgy, Cracow

^e and Heisenberg Fellow

^f now at Yale University, Dept of Physics, New Haven, USA

^g and Department of Experimental Physics, Lajos Kossuth University, Debrecen, Hungary

^h and MPI München

ⁱ now at MPI für Physik, 80805 München.

1 Introduction

The W^+W^- cross-section has been precisely measured at LEP over a range of centre-of-mass energies [1, 2], and is well described by the Standard Model (SM) expectation [3]. In this paper these measurements are extended to include also W^+W^- events with energetic photons in order to probe the modelling of electro-magnetic radiation in the W^+W^- pair creation process. No previous measurements exist of three vector boson production when at least two bosons are massive. In addition, the $W^+W^- \gamma$ final state may be sensitive to anomalous contributions to the SM $W^+W^- \gamma \gamma$ and $W^+W^- Z^0 \gamma$ quartic gauge couplings, shown in Figure 1.

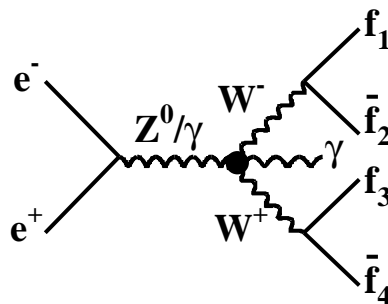


Figure 1: Standard Model $W^+W^- \gamma \gamma$ and $W^+W^- Z^0 \gamma$ quartic gauge couplings

The non-Abelian nature of the electroweak sector of the Standard Model results in vector boson self-interactions. In addition to the triple gauge boson couplings (TGCs), $W^+W^- \gamma$ and $W^+W^- Z^0$, the Standard Model predicts the existence of four quartic gauge couplings, $W^+W^- W^+W^-$, $W^+W^- Z^0 Z^0$, $W^+W^- Z^0 \gamma$ and $W^+W^- \gamma \gamma$. These couplings are not expected to play a significant role at LEP energies, but will be important at a future TeV linear collider [4] and at the LHC [5]. There has been neither direct experimental confirmation of the existence of quartic couplings, nor any direct limits on possible anomalous quartic couplings. However,

indirect limits on anomalous quartic couplings can be derived from the precise LEP/SLD Z^0 data [6, 7].

Quartic gauge boson couplings can be probed in final states with three vector bosons. At LEP centre-of-mass energies, final states involving three massive gauge bosons are kinematically out of reach. However, it is possible to study the processes $e^+e^- \rightarrow W^+W^-\gamma$ and $e^+e^- \rightarrow Z^0\gamma\gamma$. In the Standard Model, the contribution of the quartic coupling to $e^+e^- \rightarrow W^+W^-\gamma$ is expected to be too small to measure and that to $e^+e^- \rightarrow Z^0\gamma\gamma$ is zero. Nevertheless, it is possible to set the first direct limits on possible anomalous contributions to the quartic gauge boson couplings.

This paper describes a study of the process $e^+e^- \rightarrow W^+W^-\gamma$ using 183 pb $^{-1}$ of data recorded at a centre-of-mass energy of 189 GeV with the OPAL detector at LEP. It begins with an introduction to the phenomenology of quartic gauge boson couplings at LEP, followed by a description of the selection of $W^+W^-\gamma$ events and of the measurement of the $W^+W^-\gamma$ cross-section for photon energies $E_\gamma > 10$ GeV. The results are then interpreted as direct limits on possible anomalous $W^+W^-\gamma\gamma$ and $W^+W^-Z^0\gamma$ quartic gauge couplings and compared with the indirect limits.

2 Anomalous Quartic Gauge Couplings

In the Standard Model the form and strength of the vector boson self-interactions are fixed by $SU(2) \times U(1)$ gauge invariance. As is the case for triple gauge boson couplings [8], in extensions to the Standard Model, anomalous quartic couplings can be parametrised by additional terms in the Lagrangian [9, 10, 11]. These are required to conserve custodial $SU(2)_c$ symmetry in order to avoid deviations of the ρ parameter¹ from the experimentally well established value close to 1. Only operators which do not introduce anomalous triple gauge couplings are considered. For example, the anomalous quadrupole moment operator generates both $W^+W^-\gamma$ and $W^+W^-\gamma\gamma$ couplings. Therefore, it is not considered as a source of genuine anomalous quartic couplings since its strength, λ_γ , is already tightly constrained from the study of TGCs at LEP [1, 12] and at the Tevatron [13]. The lowest dimension operators which generate genuine anomalous quartic couplings involving photons are of dimension six. Three such possibilities are considered here, \mathcal{L}_6^0 , \mathcal{L}_6^c [9] and \mathcal{L}_6^n [6, 11]:

$$\begin{aligned}\mathcal{L}_6^0 &= -\frac{e^2}{16\Lambda^2}a_0F^{\mu\nu}F_{\mu\nu}\vec{W}^\alpha \cdot \vec{W}_\alpha, \\ \mathcal{L}_6^c &= -\frac{e^2}{16\Lambda^2}a_cF^{\mu\alpha}F_{\mu\beta}\vec{W}^\beta \cdot \vec{W}_\alpha, \\ \mathcal{L}_6^n &= i\frac{e^2}{16\Lambda^2}a_n\epsilon_{ijk}W_{\mu\alpha}^{(i)}W_\nu^{(j)}W^{(k)\alpha}F^{\mu\nu},\end{aligned}$$

with

$$\vec{W}_\mu = \begin{pmatrix} \frac{1}{\sqrt{2}}(W_\mu^+ + W_\mu^-) \\ \frac{i}{\sqrt{2}}(W_\mu^+ - W_\mu^-) \\ Z_\mu/\cos\theta_W \end{pmatrix},$$

where $F^{\mu\nu}$ and $W^{\mu\nu}$ are the field strength tensors of the photon and W fields respectively. Both \mathcal{L}_6^0 and \mathcal{L}_6^c , which conserve C and P (separately), generate anomalous $W^+W^-\gamma\gamma$ and $Z^0Z^0\gamma\gamma$

¹ $\rho = M_W^2/(M_{Z^0}^2 \cos^2\theta_W)$, where M_W and M_{Z^0} are the masses of the W^\pm and Z^0 bosons and θ_W is the weak mixing angle.

couplings. The CP violating term \mathcal{L}_6^n results in an anomalous $W^+W^-\gamma$ coupling². In each case, the strength of the coupling is proportional to a_i/Λ^2 , where Λ represents a scale for new physics. A more general description of the operators leading to anomalous quartic couplings accessible at LEP can be found in the recent paper of Bélanger *et al.*[14].

Figure 2a shows the predicted cross-section for $W^+W^-\gamma$ as a function of different values of a_0/Λ^2 , a_c/Λ^2 and a_n/Λ^2 , using the calculation of Stirling and Werthenbach [11]. The forms of \mathcal{L}_6^0 , \mathcal{L}_6^c and \mathcal{L}_6^n dictate that contributions to the $W^+W^-\gamma$ matrix element from the anomalous quartic couplings scale linearly with the energy of the photon [11]. The cross-section calculation of reference [11] has been used to investigate further the effects of anomalous couplings on the energy spectrum of photons in $W^+W^-\gamma$ events and on the angular distribution of the photons. For $\sqrt{s} = 189$ GeV the effects of a large anomalous coupling (*e.g.* a_0) are shown in Figure 2b and 2c. The signal of anomalous quartic gauge boson couplings at LEP would be an excess of $W^+W^-\gamma$ events with photon energy greater than 10 GeV.

3 The $W^+W^-\gamma$ Final State

There are 23 lowest order diagrams which contribute to the process $e^+e^- \rightarrow W^+W^-(\gamma) \rightarrow q\bar{q}\ell\bar{\nu}_\ell\gamma$. There are an additional 3 diagrams for the process $e^+e^- \rightarrow W^+W^-(\gamma) \rightarrow q\bar{q}q\bar{q}\gamma$. These diagrams correspond to initial state radiation (ISR), final state radiation (FSR), radiation from the W-boson (WR) and the Standard Model quartic gauge coupling (QGC) diagram. Different Monte Carlo generators and calculations employ different subsets/implementations of these diagrams. In this study, two Monte Carlo generators, WWF [16] and KORALW [17] are used to simulate the Standard Model expectation for the $W^+W^-\gamma$ final state. The WWF Monte Carlo generator produces $W^+W^-\gamma$ events above some photon energy cut and within a specified acceptance in polar angle. This program implements a full matrix element calculation for the Standard Model ISR, FSR, WR and QGC diagrams [18]. However, this treatment may not be optimal for radiation from quarks where it is also necessary to consider QCD corrections to the radiation process. Higher order corrections are implemented using a structure function approach to collinear ISR. The KORALW generator, used to simulate $W^+W^-(\gamma)$ events, does not include contributions from radiation from the intermediate W-bosons or from the Standard Model quartic coupling diagram. FSR from leptons is implemented using the PHOTOS [19] program and FSR from quarks is modelled with JETSET [20]. However, since the Standard Model $W^+W^-\gamma$ cross-section is dominated by ISR, reasonable predictions are obtained. The Monte Carlo samples generated with both WWF and KORALW are passed through the full OPAL detector simulation [21]. Neither WWF nor KORALW currently allows for anomalous quartic gauge couplings. The calculation of Stirling and Werthenbach [11] allows for the assessment of the impact of anomalous quartic couplings and is implemented in the EEWWG program. This calculation includes the ISR diagrams, the WR diagrams, the SM quartic diagram and can accommodate anomalous quartic couplings. It does not include FSR and therefore ignores any possible interference effects between the FSR diagrams and the other diagrams.

²In reference [14] it is pointed out that the form for \mathcal{L}_6^n used in [11] is missing a factor of i which is crucial for hermiticity. The missing factor of i was a typographical error in the paper. However, the implementation in the EEWWG program is correct[15].

3.1 $W^+W^-\gamma$ Signal Definition

The process $e^+e^- \rightarrow W^+W^-\gamma$ results in a four-fermion plus photon final state, $f_1\bar{f}_2f_3\bar{f}_4\gamma$, where the fermion flavours are appropriate for W-decay. Two distinct regions in phase space are considered. In the first, the $f_1\bar{f}_2$ and $f_3\bar{f}_4$ systems are produced with invariant masses close to M_W . In the second region, which is dominated by final state radiation, either the $f_1\bar{f}_2\gamma$ and $f_3\bar{f}_4$ combinations or the $f_1\bar{f}_2$ and $f_3\bar{f}_4\gamma$ combinations give invariant masses close to the W-boson mass. The second region has little sensitivity to anomalous quartic couplings. For photon energies $E_\gamma \gg \Gamma_W$, where Γ_W is the W-boson width, it is possible to separate the phase space of events from FSR from those arising from the ISR or QGC diagrams using the invariant masses of the $f_1\bar{f}_2$ and $f_3\bar{f}_4$ systems.

Both the selection procedure and the signal definition are designed to suppress contributions from FSR which is effectively a background process. The cuts used also reject photons from the decays of π^0 and η mesons associated with the hadronic jets. For this paper, the $W^+W^-\gamma \rightarrow f_1\bar{f}_2f_3\bar{f}_4\gamma$ cross-section, denoted by $\hat{\sigma}_{WW\gamma}$, is defined by:

- $|\cos\theta_\gamma| < 0.9$, where $\cos\theta_\gamma$ is the cosine of the polar angle³ of the photon.
- $\cos\theta_{\gamma f} < 0.9$, where $\cos\theta_{\gamma f}$ is the cosine of the minimum angle between the photon and any of the charged fermions in the four-fermion final state.
- $\text{minimum}(M_{f_1\bar{f}_2}, M_{f_3\bar{f}_4}) > 73 \text{ GeV}$, where $M_{f_1\bar{f}_2}$ and $M_{f_3\bar{f}_4}$ are the invariant masses of the fermions from the W^- and from the W^+ .
- $E_\gamma > 10 \text{ GeV}$, where E_γ is the photon energy.

In the above definition, all cuts are made on generator level quantities. Generator level refers to the true four-momenta of particles in the $f_1\bar{f}_2f_3\bar{f}_4\gamma$ final state. The first two cuts suppress ISR and FSR respectively and the invariant mass cuts further suppress final state radiation. The cross-section within the above kinematic cuts, $\hat{\sigma}_{WW\gamma}$, is dominated by doubly-resonant W^+W^- production. At $\sqrt{s} = 189 \text{ GeV}$, the effects of other four-fermion diagrams resulting in final states which can interfere with $W^+W^-\gamma$ have been evaluated with the RACOONWW program [22]. For the signal acceptance, the cross-section for the $e^+e^- \rightarrow W^+W^-\gamma$ diagrams alone is $109.33 \pm 0.02 \text{ fb}$ and when all (interfering) four-fermion diagrams are included this becomes $109.84 \pm 0.03 \text{ fb}$ [23], where in both cases the errors are statistical. Currently the predictions of RACOONWW do not include higher-order corrections from collinear ISR.

The Standard Model expectations for the cross-section for the $W^+W^-\gamma$ final state within this acceptance for $E_\gamma > 10 \text{ GeV}$ have been determined using the WWF and KORALW generators and the EEWWG program. The results are summarised in Table 1. Also given in Table 1 are the cross-sections from EEWWG, WWF and RACOONWW where the effect of collinear ISR has been neglected.

4 The OPAL Detector, Data and Monte Carlo Samples

The OPAL detector includes a 3.7 m diameter tracking volume within a 0.435 T axial magnetic field. The tracking detectors consist of a silicon micro-vertex detector, a high precision gas

³The OPAL right-handed coordinate system is defined such that the origin is at the centre of the detector and the z axis points along the direction of the e^- beam, θ is the polar angle with respect to the z axis.

vertex detector and a large volume gas jet chamber. Lying outside the solenoid, the electromagnetic calorimeter consisting of 11 704 lead glass blocks has full acceptance in the range $|\cos\theta| < 0.98$ and a relative energy resolution of approximately 6% for 10 GeV photons. The magnet return yoke is instrumented with streamer tubes which serve as the hadronic calorimeter. Muon chambers outside the hadronic calorimeter provide muon identification in the range $|\cos\theta| < 0.98$. A detailed description of the OPAL detector can be found in [24].

The integrated luminosity of the data sample recorded during the 1998 LEP operation, evaluated using small angle Bhabha scattering events observed in the silicon tungsten forward calorimeter [25], is $183.05 \pm 0.16(\text{stat.}) \pm 0.37(\text{sys.}) \text{ pb}^{-1}$. The luminosity-weighted mean centre-of-mass energy for the data sample is $\sqrt{s} = 188.63 \pm 0.04 \text{ GeV}$.

Both the WWF and KORALW Monte Carlo samples are used to simulate $W^+W^-\gamma$ events. Selection efficiencies are estimated using WWF. Differences between efficiencies calculated using WWF and KORALW are assigned as systematic uncertainties related to the theoretical modelling of $W^+W^-\gamma$ production, and in particular, the modelling of FSR. A number of Monte Carlo samples, all including a full simulation of the OPAL detector, are used to simulate background processes to $W^+W^-(\gamma)$. The background process $Z^0 \rightarrow q\bar{q}$ is simulated using PYTHIA [26], with HERWIG [27] and KK2F [28] used as alternatives to assess systematic uncertainties. The four-fermion backgrounds from $(Z^0/\gamma)(Z^0/\gamma)$ and $W\bar{\nu}_e$ are simulated with PYTHIA, GRC4F [29] and EXCALIBUR [30].

5 $W^+W^-\gamma$ Event Selection

The selection of $W^+W^-\gamma$ events proceeds in three stages: selection of W^+W^- events, photon identification and acceptance cuts, and kinematic requirements. Initially the energy requirement on identified photons is $E_\gamma > 5 \text{ GeV}$. However, for the determination of the $W^+W^-\gamma$ cross-section and the anomalous coupling analysis only events with photon energies $E_\gamma > 10 \text{ GeV}$ are used. The photon energy range 5-10 GeV has little sensitivity to anomalous couplings and is subject to a larger background contribution and consequently larger systematic uncertainties.

For this analysis, $W^+W^-(\gamma) \rightarrow \ell\bar{\nu}_\ell\ell\nu_\ell\gamma$ events are not used because it is not possible to reject adequately FSR photons using the kinematics of the event. However, in the determination of $\hat{\sigma}_{WW\gamma}$ the value quoted has been corrected to include all final states.

5.1 W^+W^- Selection

The $W^+W^- \rightarrow q\bar{q}\ell\bar{\nu}_\ell$ and $W^+W^- \rightarrow q\bar{q}q\bar{q}$ selections of reference [1] are used as the basis of the $W^+W^-\gamma$ selection at 189 GeV. For the selection of $W^+W^-(\gamma) \rightarrow q\bar{q}\ell\bar{\nu}_\ell\gamma$ events, the standard $W^+W^- \rightarrow q\bar{q}\ell\bar{\nu}_\ell$ selection is applied, but with one additional requirement. In a significant fraction of events selected as $W^+W^- \rightarrow q\bar{q}(\tau \rightarrow h^\pm n\pi^0\nu)\nu$ and $W^+W^- \rightarrow q\bar{q}(\tau \rightarrow 3h^\pm n\pi^0\nu)\nu$, the track(s) and clusters identified as the tau decay products are in reality associated with one of the jets. In order to reduce this contamination, the tau decay candidate track (highest momentum track in the case of 3-prong decays) is required to have momentum greater than 3 GeV. For photons with $|\cos\theta_\gamma| < 0.9$ the selection efficiency for $W^+W^-(\gamma) \rightarrow q\bar{q}\ell\bar{\nu}_\ell\gamma$ events is approximately constant at 87% in the photon energy range 10-30 GeV, and is almost independent of the polar angle of the photon within the accepted region.

For the selection of $W^+W^-(\gamma) \rightarrow q\bar{q}q\bar{q}\gamma$ events, a modified version of the $W^+W^- \rightarrow q\bar{q}q\bar{q}$ selection of reference [1] is used. In this selection events are forced into four jets using the Durham k_T algorithm [31]. In approximately 10% of Monte Carlo events with a photon with

$E_\gamma > 10$ GeV, the photon alone forms one of the four jets. This introduces an additional inefficiency, due to the requirement in the preselection that there should be at least one charged track associated with each jet. For this reason, events failing the standard $W^+W^- \rightarrow q\bar{q}q\bar{q}$ selection are forced into four jets after excluding the highest energy isolated electro-magnetic calorimeter cluster and the selection re-applied. The selection efficiency for $W^+W^- \rightarrow q\bar{q}q\bar{q}\gamma$ events with photon energies in the range 10-30 GeV is 90% and is approximately independent of the photon energy and photon polar angle.

5.2 Photon Identification and Acceptance

Photon identification is similar to that described in [32]. Photon candidates are identified as one of three types:

- Unassociated electro-magnetic calorimeter clusters defined by the requirement that no charged track lie within the angular resolution of the cluster when extrapolated to the calorimeter. The lateral spread of the cluster was required to satisfy the criteria described in reference [32].
- Two-track photon conversions which are selected using an artificial neural network.
- Conversions where only a single track is reconstructed, identified as an electro-magnetic calorimeter cluster associated with a charged track which is consistent with pointing to the primary vertex. The track is required to have no associated hits in either layer of the silicon micro-vertex detector or in the first 6 layers of the central vertex chamber. Up to one additional charged track passing the same criteria is allowed to point to the cluster.

For both types of conversions, the photon energy is defined by the sum of cluster energies pointed to by the track(s).

Photon candidates identified using the above criteria are required to satisfy isolation requirements. The energy of additional tracks and clusters in a 20° half-angle cone defined by the photon direction has to be less than 2 GeV. In addition, the energy deposited in the hadron calorimeter in a 20° half-angle cone around the photon candidate is required to be less than 5 GeV.

The identified photon is required to lie within the polar acceptance,

- $|\cos \theta_\gamma| < 0.9$.

The photon is also required to be isolated from the charged fermions in the final state. Cuts are applied on the cosine of the angle between the photon and closest jet, $\cos \theta_{\gamma\text{-JET}}$, and on the cosine of the angle between the photon and lepton, $\cos \theta_{\gamma\ell}$:

- $\cos \theta_{\gamma\text{-JET}} < 0.9$,
- $\cos \theta_{\gamma\ell} < 0.9$ for $W^+W^- \rightarrow q\bar{q}e\bar{\nu}_e\gamma$ and $W^+W^- \rightarrow q\bar{q}\mu\bar{\nu}_\mu\gamma$,
- $\cos \theta_{\gamma\ell} < 0.7$ for $W^+W^- \rightarrow q\bar{q}\tau\bar{\nu}_\tau\gamma$.

For photons within the generator level acceptance $E_\gamma > 10$ GeV, $|\cos \theta_\gamma| < 0.9$ and $\cos \theta_{\gamma f} < 0.9$, the photon identification efficiency is about 83% for selected $W^+W^-(\gamma) \rightarrow q\bar{q}\ell\bar{\nu}_\ell\gamma$ and $W^+W^-(\gamma) \rightarrow q\bar{q}q\bar{q}\gamma$ events.

5.3 Kinematic Requirements

Kinematic cuts which reject events with FSR photons or with photons associated with the hadronic jets, *i.e.* from π^0 and η decays, are performed by comparing the results of three kinematic fits. In each case, the constraints of energy and momentum conservation are imposed. The finite W width is neglected and the two reconstructed masses of the W boson candidates are required to be equal [33]. The fits employed correspond to the following hypotheses:

- a) FSR(quark), assuming a two-body W^+W^- final state, where the identified photon is associated with one of the jets.
- b) FSR(lepton), only used for $W^+W^-(\gamma) \rightarrow q\bar{q}\ell\bar{\nu}_\ell\gamma$ events, assuming a two-body W^+W^- final state, where the photon is associated with the charged lepton.
- c) ISR/QGC, assuming a three body final state consisting of two W bosons and the photon.

An event is considered consistent with one of the above fit hypotheses if the fit converges with a fit probability of greater than 0.1% and if the reconstructed W boson mass is greater than 74 GeV. Only $W^+W^-\gamma$ candidate events consistent with being two approximately on-shell W -bosons (fit c), $M_{f_1\bar{f}_2} \sim M_{f_3\bar{f}_4} \sim M_W$, are retained for the measurement of the $W^+W^-\gamma$ cross-section and quartic gauge coupling study. This procedure suppresses events with final state radiation and events where the photon is from the decay of mesons. By reducing contamination from FSR, the sensitivity to anomalous quartic couplings is improved. In addition, the systematic uncertainties from photons associated with jets (FSR and π^0/η decays) are significantly reduced.

Selected $W^+W^-(\gamma) \rightarrow q\bar{q}\ell\bar{\nu}_\ell\gamma$ events are required to be consistent with the ISR/QGC hypothesis using the above criteria. The effect of the invariant mass cut is indicated in Figure 3. In order further to reduce contributions from FSR, if the event is also consistent with the hypothesis of FSR from the lepton, it is required that the reconstructed mass from the ISR/QGC fit be closer to M_W than the mass obtained from the FSR(lepton) fit.

In fully hadronic events there are three possible jet-pairing combinations. Only events where one of the three combinations is kinematically consistent with the ISR/QGC hypothesis are retained. If more than one combination satisfies this requirement, the fit yielding the highest probability is used. Events which are also consistent with the FSR(quark) hypothesis are rejected if the FSR fit has higher probability than the ISR/QGC fit and if $M_{\text{FSR}} < 86$ GeV and $M_{\text{ISR}} < 78$ GeV, where M_{FSR} and M_{ISR} are the respective reconstructed masses.

The application of the above kinematic requirements retains approximately 80% of $W^+W^-\gamma$ events within the signal definition of Section 3.1 whilst rejecting 85%-98% (increasing with the photon energy) of events with photons from FSR or from the decays of mesons.

6 $W^+W^-\gamma$ cross-section

Using the selection criteria defined in the previous section, 17 $W^+W^-\gamma$ events with $E_\gamma > 10$ GeV are selected compared to the Monte Carlo expectation⁴ of 13.2 events. Figure 4a shows the photon energy spectrum for the selected $W^+W^-\gamma$ event sample at $\sqrt{s} = 189$ GeV. Also shown are the data for photon energies in the range 5 – 10 GeV. One event is observed

⁴Here KORALW was used for the expectation from $W^+W^-(\gamma)$ and PYTHIA was used to simulate the backgrounds from $q\bar{q}$, Z^0Z^0 and $W\ell\bar{\nu}_\ell$.

with $E_\gamma > 30$ GeV, compared to the expectation of 0.1. This event occurs in the electromagnetic calorimeter barrel/endcap overlap region where the energy resolution is relatively poor. Figure 4b shows the distribution of $\cos \theta_\gamma$ for the events with $E_\gamma > 10$ GeV and Figure 4c shows the distribution of the cosine of the angle between the photon and nearest charged fermion in the event. Good agreement between data and Monte Carlo is observed.

New physics could appear as resonant structure in the $W\gamma$ invariant mass distribution. To investigate this possibility, the invariant masses of the two $W^\pm\gamma$ combinations in selected $W^+W^-\gamma$ events are obtained from an additional kinematic fit. The fit uses the constraints of energy and momentum conservation and the constraint that the invariant masses of the reconstructed, $f_1\bar{f}_2$ and $f_3\bar{f}_4$ systems are both equal to the W-mass. Only events for which the kinematic fit converges are retained. The $W\gamma$ invariant mass is calculated from the four-momenta of the four fermions and the photon returned by the fit. Figure 5 shows the reconstructed invariant mass distribution for the two $W^\pm\gamma$ combinations for selected $W^+W^-\gamma$ events with $E_\gamma > 5$ GeV. No resonant structure is observed.

The $W^+W^-\gamma$ cross-section for $E_\gamma > 10$ GeV is determined within the acceptance defined in Section 3.1. The selection efficiency for events within this acceptance, $\varepsilon_{WW\gamma}$, is evaluated using the WWF Monte Carlo sample. Backgrounds from $q\bar{q}(\gamma)$ and Z^0Z^0 are estimated using PYTHIA. The background from W^+W^- events with a fake photon from the electro-magnetic decays of mesons is estimated using KORALW. These three sources are summed to form the total non- $W^+W^-\gamma$ background, σ_{BGD} . Due to the steeply falling photon energy spectrum, the effect of the finite photon energy resolution is that more events from lower energies are reconstructed with $E_\gamma > 10$ GeV than vice versa. A correction, c_{res} , is applied to account for this migration. In addition, it is necessary to account for accepted $W^+W^-\gamma$ events from outside the invariant mass region used to define the cross-section using a correction factor, $P_{WW\gamma}$, which is defined as the fraction of accepted $f_1\bar{f}_2f_3\bar{f}_4\gamma$ events which have $M_{f_1\bar{f}_2} > 73$ GeV and $M_{f_3\bar{f}_4} > 73$ GeV. The $W^+W^-\gamma$ cross-section is calculated from

$$\hat{\sigma}_{WW\gamma} = \frac{P_{WW\gamma}(N_{obs} - \sigma_{BGD}\mathcal{L})}{\varepsilon_{WW\gamma}c_{res}\mathcal{L}},$$

where N_{obs} is the accepted number of events with $E_\gamma > 10$ GeV and \mathcal{L} is the integrated luminosity. The values of the quantities used to determine the cross-section and associated uncertainties are listed in Table 2, giving the result,

$$\hat{\sigma}_{WW\gamma} = 136 \pm 37 \pm 8 \text{ fb},$$

where the first error is statistical and the second systematic. This result is consistent with the expectations (85 – 102 fb) of the WWF, KORALW and EEWWG presented in Table 1. The sources of systematic uncertainty, summarised in Table 3, are described below.

6.1 Systematic Uncertainties

W⁺W⁻ Selection Efficiency: The systematic uncertainty on the selection of W^+W^- events is estimated to be 0.9%. This estimate was obtained in a manner similar to that described in [1]. The largest uncertainties are related to the QCD and fragmentation modelling of jets.

Photon Identification: A systematic uncertainty of 1% is assigned to cover the uncertainties in the simulation of the photon conversion rate and the accuracy of the simulation of the electromagnetic cluster shape.

Photon Isolation: The systematic error associated with the isolation requirements depends on the accuracy of the Monte Carlo simulation of the fragmentation process in hadronic jets. This is verified in $Z^0 \rightarrow q\bar{q}$ events recorded at $\sqrt{s} = 91$ GeV during the 1998 run. For each selected event, the inefficiency of the isolation requirements is determined for random orientations of the isolation cone and parametrised as a function of the angle between the cone and the nearest jet. For all jet-cone angles the inefficiency in the Monte Carlo and data agree to better than 1%, consequently a 1% systematic error is assigned.

Kinematic Fits: The $W^+W^-\gamma$ event selections require that a kinematic fit converges and has a reasonable probability. Possible mis-modelling of the detector response/resolution could result in a difference in the rates at which the fits fail for data and Monte Carlo. This was checked by applying the kinematic fits used in the W mass analysis to all selected W^+W^- events and comparing the failure rates for data and Monte Carlo. The difference in efficiency, $1.2 \pm 0.8\%$, is used as an estimate the systematic error associated with the kinematic fits.

ECAL energy scale and resolution: The systematic error (2.5%) on the correction factor, c_{res} , which accounts for feed-through from lower energy photons, is estimated by varying the electro-magnetic calorimeter energy resolution by $\pm 25\%$ and by varying the electro-magnetic calorimeter scale by $\pm 1\%$. These variations were obtained by studying photons in $e^+e^- \rightarrow \gamma\gamma$ and $e^+e^- \rightarrow e^+e^-\gamma$ at $\sqrt{s} \sim M_{Z^0}$ and $\sqrt{s} = 189$ GeV, and by studying the energy response to electrons.

Modelling of photons from jets: The modelling of photon candidates associated with the hadronic jets (both from FSR and from π^0 and η decays) is studied by comparing the rate at which photons are identified in $Z^0 \rightarrow q\bar{q}$ events from the 1998 calibration data ($\sqrt{s}=91.2$ GeV) to the PYTHIA prediction. For $10 \text{ GeV} < E_\gamma < 20 \text{ GeV}$, there are 40% more photon candidates identified in the data than expected from the Monte Carlo. Above 20 GeV the data are consistent with the Monte Carlo expectation. The ratio of data to Monte Carlo is used to estimate an energy-dependent correction to the Monte Carlo expectation for the background from W^+W^- events with fake photons. The size of this correction is assigned as a systematic uncertainty.

ISR Modelling in $q\bar{q}\gamma$ Background: The dominant source of non- W^+W^- background is from $e^+e^- \rightarrow Z^0/\gamma \rightarrow q\bar{q}\gamma$ where the identified photon is a genuine photon from ISR. The accuracy of the simulation of initial state radiation with $|\cos \theta_\gamma| < 0.9$ is studied using identified ISR photons in multi-hadronic events [34] recorded at $\sqrt{s} = 189$ GeV. A kinematic fit is used to reject events with additional radiation along the beam direction. In the range of photon energies of relevance to the $W^+W^-\gamma$ analysis, $5 \text{ GeV} < E_\gamma < 50 \text{ GeV}$, the fractions of events with an identified photon in data and Monte Carlo agree to better than 20% which is assigned as a systematic uncertainty.

Four-fermion Background: For the $W^+W^-\gamma$ cross-section measurement PYTHIA is used to estimate the background from Z^0Z^0 and single W production ($W e\bar{\nu}_e$). This four-fermion background estimate was compared to that obtained using GRC4F and EXCALIBUR. The largest difference is used to assign a systematic error.

$W^+W^-\gamma$ events from outside the signal definition: In order to account for accepted $W^+W^-\gamma$ events from outside the cross-section signal definition, a correction factor is used. This factor, $P_{WW\gamma}$, is determined to be $(85.3 \pm 0.7)\%$ from WWF and $(85.0 \pm 1.0)\%$ from

KORALW. The WWF value is taken as the central value. The comparison of these generators is sensitive to uncertainties in the treatment of FSR. Although no discrepancy is observed, the statistical error on the difference is taken as a systematic error (1.2%). In addition, a systematic uncertainty of 1.5% is assigned to account for the differences between data and Monte Carlo in the modelling of photons from jets, described previously.

7 Limits on Anomalous Quartic Couplings

The selected $W^+W^-\gamma$ events are used to set limits on possible anomalous contributions to the $W^+W^-\gamma\gamma$ and $W^+W^-Z^0\gamma$ quartic gauge couplings. The limits are extracted from the measured differential cross-section as a function of the photon energy and photon polar angle.

There is currently no Monte Carlo available that implements anomalous quartic couplings and has contributions from all Standard Model diagrams. The expected differential $W^+W^-\gamma$ cross-sections are obtained using the EEWWG program which allows for anomalous quartic couplings. Since FSR is not implemented in EEWWG it is included as an additional background process. The Monte Carlo treatment of signal and background is described below.

7.1 $W^+W^-\gamma$ Signal

The EEWWG calculation is used to determine the expected contribution from the ISR, WR, Standard Model QGC and anomalous QGC diagrams within the signal definition of Section 3.1. The only detector effect that is included is a Gaussian smearing associated with the energy resolution for the photon. No smearing was applied to the photon or fermion angles since these are relatively well measured. The selection efficiency is estimated (for events within the signal acceptance cuts) from the WWF Monte Carlo and is parametrised as a function of photon energy. The small dependence of the selection efficiency on $\cos\theta_\gamma$ is neglected in the determination of the limits on anomalous couplings. The validity of this procedure is verified using a small sample of fully-simulated Monte Carlo events generated using the EEWWG calculation.

The contribution to the cross-section from any anomalous coupling increases rapidly with centre-of-mass energy due to the additional phase space for higher energy photons. Thus the contribution to the $W^+W^-\gamma$ cross-section from anomalous QGCs is sensitive to higher-order QED radiative corrections. The EEWWG calculation currently only includes $W^+W^-\gamma$ final states. For the case of the QGC diagram, it therefore neglects the effect of additional ISR which reduces the average effective centre-of-mass energy, $\sqrt{s'}$. The effect of collinear ISR from both the electron and positron has been incorporated into the EEWWG calculation using the collinear radiator function from EXCALIBUR. At $\sqrt{s} = 189$ GeV, QED radiative corrections reduce the cross-section from anomalous QGCs by 26%.

7.2 Background Treatment

The contribution from FSR is estimated using KORALW, with FSR photons being identified using the Monte Carlo generator information. KORALW is also used to estimate the contribution from other diagrams producing final states outside the signal definition of Section 3.1. Neglecting the contribution of anomalous couplings to events outside the signal definition not only results in conservative limits but reduces the possible effects of interference with Standard Model FSR diagrams. Background from W^+W^- with a fake photon is calculated using

the corrected background from KORALW. Similarly, the four-fermion and $q\bar{q}$ backgrounds are estimated using PYTHIA. Table 4 summarises the background contributions used in the anomalous coupling study. In the table, the $W^+W^-\gamma$ background has been divided into that from ISR (outside the signal definition mass and/or acceptance cuts) and that from FSR.

7.3 Results

For the case of Standard Model quartic gauge couplings, the expected photon energy spectrum for selected events estimated using the above procedure is shown in Figure 4a. The spectrum is in reasonable agreement with that obtained from the WWF generator. By combining the predicted cross-sections from EEWWG and the backgrounds from Table 4 the expected distributions corresponding to non-zero anomalous coupling parameters can be generated. Figure 6 shows the expected photon energy distributions for two values of the anomalous coupling a_0/Λ^2 (in addition to the Standard Model prediction).

To set limits on possible anomalous couplings a binned maximum likelihood fit to the observed distribution of $[E_\gamma, \cos\theta_\gamma]$ is performed using bins of $[5 \text{ GeV}, 0.1]$, with the fit range restricted to $E_\gamma > 10 \text{ GeV}$. The 95% confidence level upper limits on the anomalous couplings are obtained from the resulting likelihood curves:

$$\begin{aligned} -0.070 \text{ GeV}^{-2} &< a_0/\Lambda^2 < 0.070 \text{ GeV}^{-2}, \\ -0.13 \text{ GeV}^{-2} &< a_c/\Lambda^2 < 0.19 \text{ GeV}^{-2}, \\ -0.61 \text{ GeV}^{-2} &< a_n/\Lambda^2 < 0.57 \text{ GeV}^{-2}. \end{aligned}$$

The expected 95% confidence level upper limit on a_0/Λ^2 is 0.045. These limits from the data are higher than the expected limits due to the slight excess of high energy photons in the data. The probability of obtaining a limit greater than or equal to the observed limit is approximately 2%. The limits were derived including the systematic uncertainties described in the previous section. For these results, a 15% theoretical uncertainty on the cross-section normalisation of the EEWWG calculation is assumed.

These are the first direct limits on anomalous quartic couplings. However, indirect limits can be derived from radiative corrections to LEP/SLD Z^0 data. The experimental limits on deviations of the S,U,T parameters [35] (or equivalently $\epsilon_1, \epsilon_2, \epsilon_3$ [36]) from their Standard Model values has been used to place constraints on the anomalous $W^+W^-\gamma\gamma$ and $Z^0Z^0\gamma\gamma$ couplings [6]: $-0.0007 < a_0/\Lambda^2 < 0.0001$ and $-0.0017 < a_c/\Lambda^2 < 0.0009$. However, these indirect limits are obtained under a restrictive set of assumptions and their validity has been questioned [14]. There are currently no limits on a_n corresponding to an anomalous $W^+W^-Z^0\gamma$ coupling.

8 Conclusions

The first study of $W^+W^-\gamma$ events produced in e^+e^- collisions is presented. From the seventeen selected events with $E_\gamma > 10 \text{ GeV}$, the $W^+W^-\gamma$ production cross-section is measured to be:

$$\hat{\sigma}_{WW\gamma} = 136 \pm 37 \pm 8 \text{ fb},$$

within the $f_1\bar{f}_2f_3\bar{f}_4\gamma$ generator level acceptance defined by $|\cos\theta_\gamma| < 0.9$, $\cos\theta_{\gamma f} < 0.9$ and $M_{f_1\bar{f}_2}, M_{f_3\bar{f}_4} > 73 \text{ GeV}$, in agreement with Standard Model expectation.

The distribution of the photon energy and polar angle is used to set limits on possible anomalous contributions to the $W^+W^-\gamma\gamma$ and $W^+W^-\gamma Z^0$ vertices:

$$\begin{aligned} -0.070 \text{ GeV}^{-2} &< a_0/\Lambda^2 < 0.070 \text{ GeV}^{-2}, \\ -0.13 \text{ GeV}^{-2} &< a_c/\Lambda^2 < 0.19 \text{ GeV}^{-2}, \\ -0.61 \text{ GeV}^{-2} &< a_n/\Lambda^2 < 0.57 \text{ GeV}^{-2}, \end{aligned}$$

where Λ represents the energy scale for new physics. These are the first direct limits on anomalous quartic couplings.

9 Acknowledgements

We would like to thank James Stirling and Anja Werthenbach for providing the program EEWWG which is used to determine the effects of anomalous couplings in $W^+W^-\gamma$ events. We also greatly appreciate their many useful suggestions and comments. We would also like to thank Markus Roth and Doreen Wackerroth and for providing the $4f\gamma$ cross-section calculations using the RACOONWW program. We thank Fawzi Boudjema for his comments on this paper and for useful discussions.

We particularly wish to thank the SL Division for the efficient operation of the LEP accelerator at all energies and for their continuing close cooperation with our experimental group. We thank our colleagues from CEA, DAPNIA/SPP, CE-Saclay for their efforts over the years on the time-of-flight and trigger systems which we continue to use. In addition to the support staff at our own institutions we are pleased to acknowledge the

Department of Energy, USA,

National Science Foundation, USA,

Particle Physics and Astronomy Research Council, UK,

Natural Sciences and Engineering Research Council, Canada,

Israel Science Foundation, administered by the Israel Academy of Science and Humanities,

Minerva Gesellschaft,

Benozziyo Center for High Energy Physics,

Japanese Ministry of Education, Science and Culture (the Monbusho) and a grant under the Monbusho International Science Research Program,

Japanese Society for the Promotion of Science (JSPS),

German Israeli Bi-national Science Foundation (GIF),

Bundesministerium für Bildung, Wissenschaft, Forschung und Technologie, Germany,

National Research Council of Canada,

Research Corporation, USA,

Hungarian Foundation for Scientific Research, OTKA T-029328, T023793 and OTKA F-023259.

References

- [1] OPAL Collaboration, G. Abbiendi *et al.*, Eur. Phys. J. **C8** (1999) 191.
- [2] ALEPH Collaboration, R. Barate *et al.*, Phys. Lett. **B453** (1999) 107;
DELPHI Collaboration, P. Abreu *et al.*, Phys. Lett. **B456** (1999) 310;
L3 Collaboration, M. Acciarri *et al.*, Phys. Lett. **B436** (1998) 437.
- [3] D. Bardin *et al.*, Nucl. Phys. B, Proc. Suppl. **37B** (1994) 148;
D. Bardin *et al.*, Comp. Phys. Comm. **104** (1997) 161.
- [4] E. Boos, H.-J. He, W. Kilian, A. Pukhov, C.-P. Yuan and P.M. Zerwas, “Strongly Interacting Vector Bosons at TeV $e^{\pm}e^{-}$ Linear Colliders”, DESY-96-256, hep-ph/9708310.
- [5] A.S. Belyaev, O.J.P. Eboli, M.C. Gonzalez-Garcia, J.K. Mizukoshi, S.F. Novaes and I. Zacharov, Phys. Rev. **D59** (1999) 015022.
- [6] O.J.P. Eboli, M.C. González-Garcia and S.F. Novaes, Nucl. Phys. **B411** (1994) 381.
- [7] A. Brunstein, O.J.P. Eboli and M.C. Gonzalez-Garcia, Phys. Lett. **B375** (1996) 233.
- [8] K. Hagiwara, R.D. Peccei, D. Zeppenfeld and K. Hikasa, Nucl. Phys. **B282** (1987) 253.
- [9] G. Bélanger and F. Boudjema, Phys. Lett. **B288** (1992) 201.
- [10] G. Abu Leil and W.J. Stirling, J. Phys. **G21** (1995) 517.
- [11] W.J. Stirling and A. Werthenbach, DTP-99-30, hep-ph/9903315, to be published in Eur. Phys. J. **C**.
- [12] ALEPH Collaboration, R. Barate *et al.*, Phys. Lett. **B422** (1998) 369;
DELPHI Collaboration, P. Abreu *et al.*, Phys. Lett. **B459** (1999) 382;
L3 Collaboration, M. Acciarri *et al.*, Phys. Lett. **B413** (1997) 176.
- [13] CDF Collaboration, F. Abe *et al.*, Phys. Rev. Lett. **78** (1997) 4536;
D0 Collaboration, B. Abbott *et al.*, Phys. Rev. **D58** (1998) 051101.
- [14] G. Bélanger, F. Boudjema, Y. Kurihara, D. Perret-Gallix and A. Semenov, “Bosonic Quartic Couplings at LEP2”, KEK-CP-087, LAPTH-744/99, hep-ph/9908254 (1999).
- [15] A. Werthenbach, private communication.
- [16] G.J. van Oldenborgh, P.J. Franzini and A. Borrelli, Comp. Phys. Comm. **83** (1994) 14.
- [17] Program KORALW V1.42, M. Skrzypek *et al.*, Comp. Phys. Comm. **94** (1996) 216;
M. Skrzypek *et al.*, Phys. Lett. **B372** (1996) 289;
M. Skrzypek *et al.*, Comp. Phys. Comm. **119** (1999) 1.
- [18] A. Aeppli and D. Wyler, Phys. Lett. **B262** (1991) 125.
- [19] E. Barberio and Z. Was, Comp. Phys. Comm. **79** (1994) 291.
- [20] T. Sjöstrand, Comp. Phys. Comm. **39** (1986) 374;
T. Sjöstrand and M. Bengtsson, Comp. Phys. Comm. **43** (1987) 367.

- [21] J. Allison et al., Nucl. Instr. and Meth. **A317** (1992) 47.
- [22] A. Denner, S. Dittmaier, M. Roth and D. Wackeroth, “Predictions for all processes $e^+e^- \rightarrow 4$ fermions + γ ”, BI-TP 99/10, PSI-PR-99-12, hep-ph/9904472, to be published in Nucl. Phys. B.
- [23] M. Roth and D. Wackeroth, Private Communication.
- [24] OPAL Collaboration, K. Ahmet *et al.*, Nucl. Instr. and Meth. **A305** (1991) 275;
B.E. Anderson *et al.*, IEEE Transactions on Nuclear Science, **41** (1994) 845;
S. Anderson *et al.*, Nucl. Instr. and Meth. **A403** (1998) 326.
- [25] OPAL Collaboration, G. Abbiendi *et al.*, CERN-EP/99-097, Submitted to Eur. Phys. J. C.
- [26] T. Sjöstrand, Comp. Phys. Comm. **82** (1994) 74.
- [27] G. Marchesini et al., Comp. Phys. Comm. **67** (1992) 465.
- [28] S. Jadach, B.F. Ward and Z. Was, Phys. Lett. **B449** (1999) 97.
- [29] J. Fujimoto *et al.*, Comp. Phys. Comm. **100** (1997) 128.
- [30] F.A. Berends, R. Pittau and R. Kleiss, Comp. Phys. Comm. **85** (1995) 437.
- [31] N. Brown and W.J. Stirling, Phys. Lett. **B252** (1990) 657;
S. Bethke, Z. Kunszt, D. Soper and W.J. Stirling, Nucl. Phys. **B370** (1992) 310;
S. Catani *et al.*, Phys. Lett. **B269** (1991) 432;
N. Brown and W.J. Stirling, Z. Phys. **C53** (1992) 629.
- [32] OPAL Collaboration, K. Ackerstaff *et al.*, Phys. Lett. **B437** (1998) 218.
- [33] OPAL Collaboration, K. Ackerstaff *et al.*, Eur. Phys. J. **C1** (1998) 395.
- [34] OPAL Collaboration, K. Ackerstaff *et al.*, Eur. Phys. J. **C6** (1999) 1.
- [35] M.E. Peskin and T. Takeuchi, Phys. Rev. **D46** (1992) 381.
- [36] G. Altarelli, R. Barbieri and F. Caravaglios, Phys. Lett. **B349** (1995) 145.

Program	Collinear ISR	$\hat{\sigma}_{\text{WW}\gamma}$
KORALW	yes	102.4 ± 2.2 fb
EEWWG	yes	85.5 ± 0.4 fb
WWF	yes	89.3 ± 0.6 fb
EEWWG	no	106.1 ± 0.4 fb
WWF	no	110.3 ± 0.6 fb
RACONWW	no	109.33 ± 0.02 fb

Table 1: Standard Model cross-sections for the process $e^+e^- \rightarrow W^+W^-\gamma$ within the $f_1\bar{f}_2f_3\bar{f}_4\gamma$ generator level acceptance defined by $E_\gamma > 10$ GeV, $|\cos\theta_\gamma| < 0.9$, $\cos\theta_{\gamma f} < 0.9$ and $M_{f_1\bar{f}_2}, M_{f_3\bar{f}_4} > 73$ GeV. Where possible, values are quoted corresponding to the cases with and without collinear ISR.

Quantity	Value
N_{obs}	17
\mathcal{L}	183.1 ± 0.6 pb $^{-1}$
$\varepsilon_{\text{WW}\gamma}$	$48.7 \pm 1.8\%$
c_{res}	1.065 ± 0.026
σ_{BGD}	9.9 ± 2.0 fb
$P_{\text{WW}\gamma}$	$85.3 \pm 1.9\%$

Table 2: Values of the quantities used in the determination of the $W^+W^-\gamma$ cross-section. The errors include components from Monte Carlo statistics and systematic uncertainties.

Source	$\Delta\hat{\sigma}_{\text{WW}\gamma}$
W^+W^- Event Selection	3.0 fb
$q\bar{q}\gamma$ efficiency	0.5 fb
Photon Identification	1.6 fb
Photon Isolation	1.6 fb
Kinematic Fits	1.6 fb
ECAL energy scale	1.8 fb
ECAL energy resolution	2.8 fb
Photons from jets	2.7 fb
ISR modelling $q\bar{q}\gamma$	1.9 fb
Acceptance Cuts	2.8 fb
Four-fermion Events	2.0 fb
$P_{\text{WW}\gamma}$	3.0 fb
Total	7.7 fb

Table 3: Contributions to the systematic error on $\hat{\sigma}_{\text{WW}\gamma}$.

E_γ Range	non- $W^+W^-\gamma$ Background			$W^+W^-\gamma$ Background		
	W^+W^-	$4f$	$q\bar{q}$	ISR	FSR(lepton)	FSR(quark)
10 – 15 GeV	0.36 ± 0.08	0.08 ± 0.03	0.32 ± 0.08	0.29 ± 0.05	1.66 ± 0.30	0.74 ± 0.14
15 – 20 GeV	0.19 ± 0.06	0.10 ± 0.04	0.26 ± 0.07	0.25 ± 0.05	0.15 ± 0.04	0.36 ± 0.06
20 – 25 GeV	0.05 ± 0.03	0.02 ± 0.01	0.16 ± 0.05	0.06 ± 0.03	0.01 ± 0.01	0.01 ± 0.01
25 – 30 GeV	0.04 ± 0.02	0.04 ± 0.02	0.07 ± 0.03	0.00 ± 0.01	—	0.11 ± 0.04
30 – 35 GeV	0.00 ± 0.01	—	0.02 ± 0.02	—	—	0.01 ± 0.01

Table 4: Expected numbers of background events used in the anomalous coupling analysis. The W^+W^- background consists of events with a photon from the decays of a π^0 , η *etc.* In addition, $W^+W^-\gamma$ events from FSR diagrams are considered as background and estimated using KORALW. Accepted $W^+W^-\gamma$ events from outside the invariant mass cuts of the cross-section signal definition are also treated as background (denoted ISR). The quoted errors include systematic contributions.

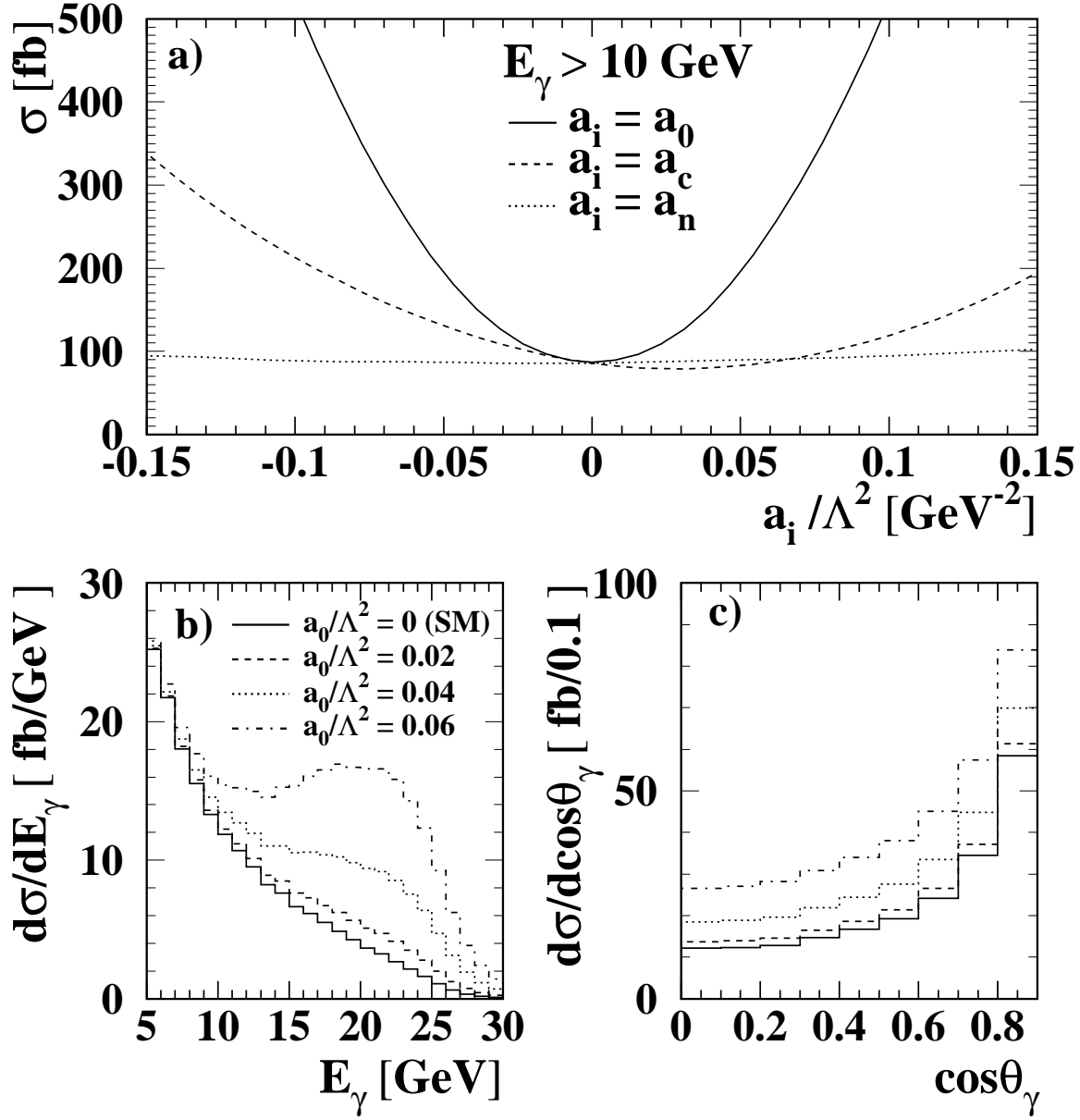


Figure 2: The effect of anomalous quartic couplings in e^+e^- collisions at $\sqrt{s} = 189$ GeV. a) Expected $W^+W^-\gamma$ cross-section for different anomalous quartic couplings, the photon was required to have energy, $E_\gamma > 10$ GeV and be within the polar acceptance, $|\cos\theta_\gamma| < 0.9$. The kinematic cuts used to define the cross-section, see text, were also applied. Plots b) and c) show the effect of an anomalous quartic gauge coupling, a_0 , on the energy and angular distribution of photons in $W^+W^-\gamma$ events, where the fiducial cuts, $E_\gamma > 5$ GeV and $|\cos\theta_\gamma| < 0.9$ were imposed. In all three figures, the contribution from final state radiation diagrams is not included.

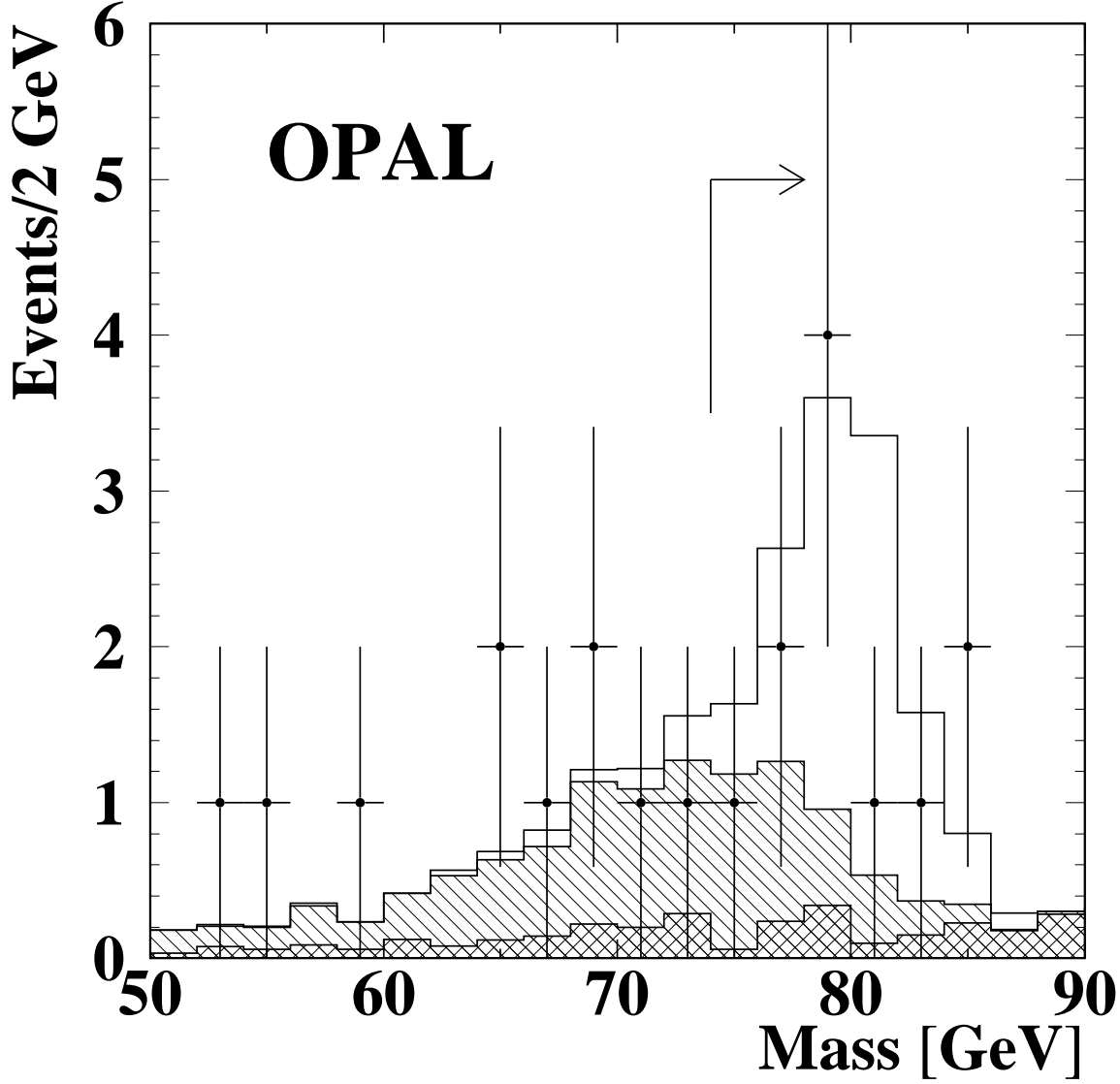


Figure 3: The reconstructed W-boson mass distribution for candidate $W^+W^-(\gamma) \rightarrow q\bar{q}l\bar{\nu}_l\gamma$ events using the ISR/QGC hypothesis. The points show the data. The histogram shows the Monte Carlo expectation where KORALW has been used to simulate the $W^+W^-(\gamma)$ final state and PYTHIA is used to simulate non- W^+W^- background. The hatched histogram shows the contribution from W^+W^- events with final state radiation or where the photon candidate originates from the decay of a meson. The double-hatched histogram shows the contribution from non- W^+W^- background. The cut is indicated by the arrow.

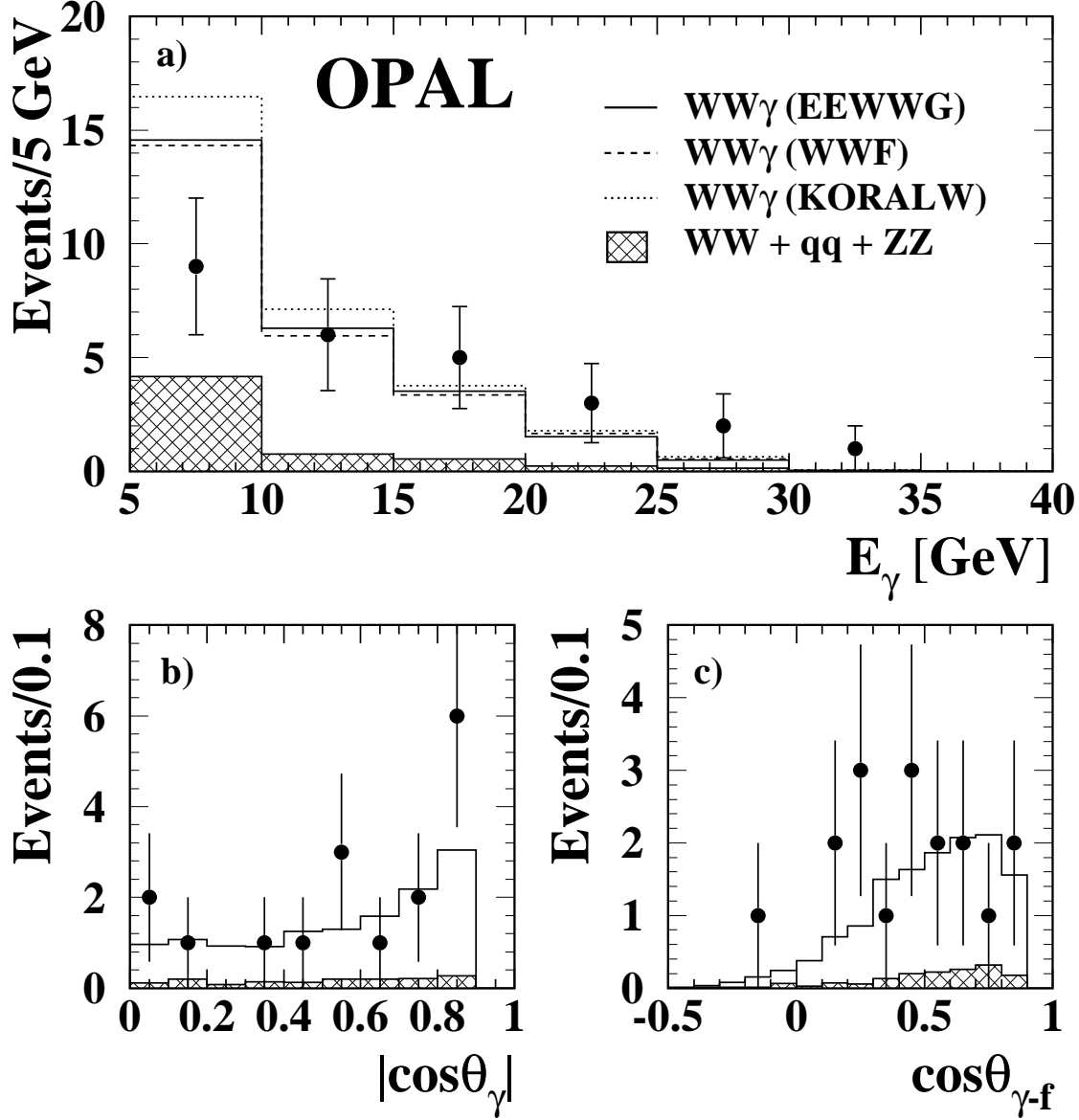


Figure 4: For selected $W^+W^-\gamma$ events, a) shows the photon energy spectrum, b) the cosine of the polar angle of the photon, and c) the cosine of the angle between the photon and the nearest fermion. In b) and c) the cut $E_\gamma > 10$ GeV has been applied. The 189 GeV data are shown by the points with error bars and the total SM Monte Carlo expectation shown by the histogram. The hatched histograms indicate the contribution from non- W^+W^- background and from fake photons in selected W^+W^- events. In Figure a) the predictions from KORALW are compared to those from WWF and EEWWG. The prediction of EEWWG also includes the estimated contribution from FSR obtained using the KORALW generator.

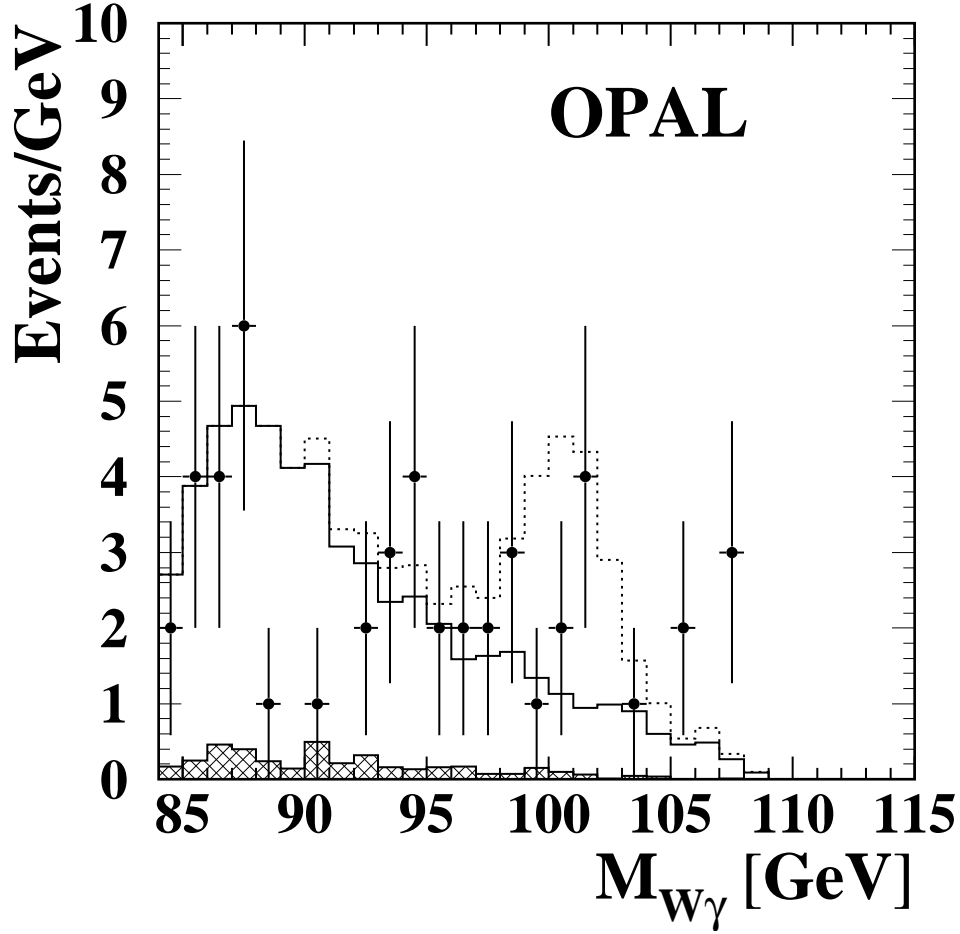


Figure 5: Reconstructed invariant mass of $W^\pm\gamma$ in selected $W^+W^-\gamma$ events with $E_\gamma > 5$ GeV (two entries per event). The 189 GeV data are shown by the points, the Standard Model expectation, determined from KORALW and PYTHIA is shown by the histogram. The shaded histogram shows the non- $W^+W^-(\gamma)$ background. Also shown, by the dotted histogram, is the expected reconstructed mass distribution (arbitrary normalisation) for a narrow resonance of mass 100 GeV which decays to $W\gamma$.

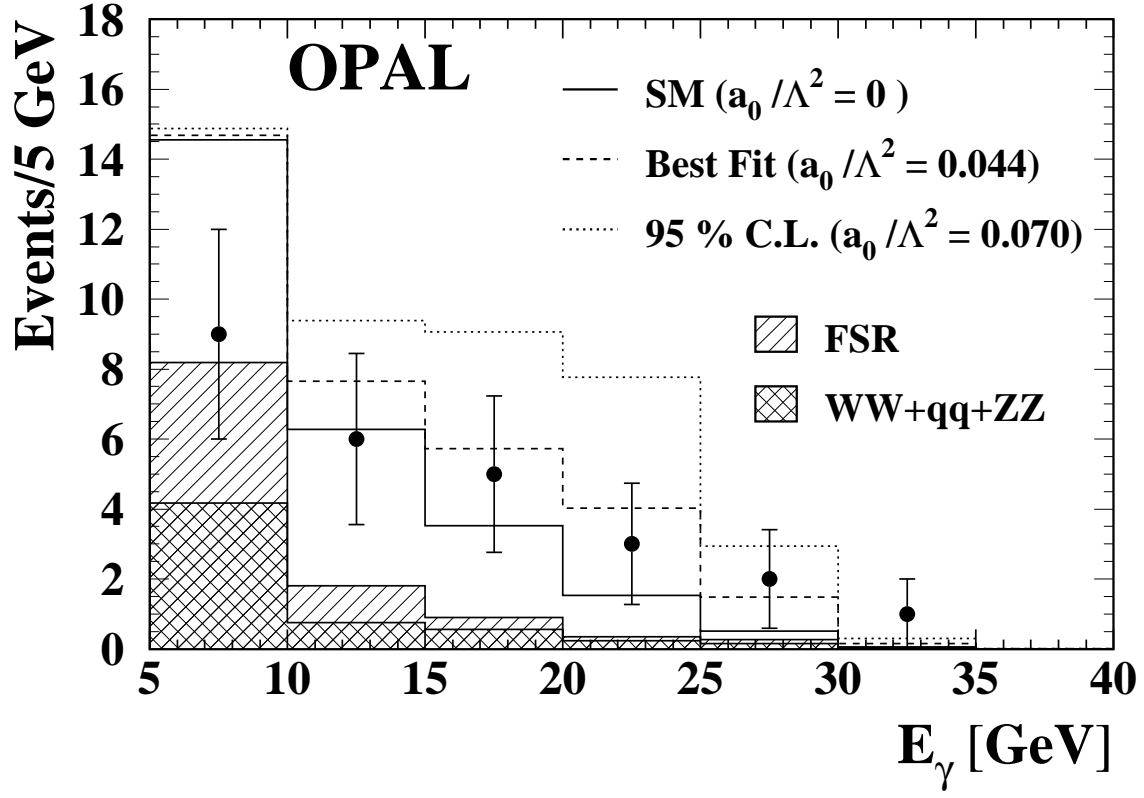


Figure 6: Energy spectrum of photons in candidate $W^+W^-\gamma$ events. The data, shown by the points with error bars, are compared to the expected distributions for three different values of the anomalous coupling a_0/Λ^2 ; the Standard Model value $a_0/\Lambda^2 = 0$, the best fit value $a_0/\Lambda^2 = 0.044$ and the distribution corresponding to the 95% confidence limit value of $a_0/\Lambda^2 = 0.070$. The double hatched histogram shows the background from non- W^+W^- events and from W^+W^- events with a fake photon. The singly hatched histogram shows the contribution from final state radiation.